How Stability of Hybrid Coupler Characteristic Affects Front-End Isolation of In-Band Full Duplex System

Soheyl Soodmand
dept.electrical & electronic engineering
university of bristol
Bristol, United Kingdom
soheyl.soodmand@bristol.ac.uk

Kevin A. Morris
dept.electrical & electronic engineering
university of bristol
Bristol, United Kingdom
kevin.morris@bristol.ac.uk

Mark A. Beach
dept.electrical & electronic engineering
university of bristol organization
Bristol, United Kingdom
m.a.beach@bristol.ac.uk

***Abstract*— In In-Band Full Duplex (IBFD) transceivers, Electrical Balance Duplexers (EBDs) provide Transmit (TX)-Receive (RX) isolation to implement a form of self-interference (SI) cancellation to facilitates simultaneous transmission and reception from a single antenna. EBD works by coupling transmitter, receiver, antenna, and balancing impedance using a hybrid coupler. The balancing impedance in the EBD needs to be equal as much as possible to the antenna impedance to achieve a high isolation while the antenna impedance variations limit the isolation bandwidth. Hybrid couplers are also not ideal elements, and their S parameters are variable in frequency domain. An antenna with a stable impedance, designed by authors, has been connected in this work to two different hybrid couplers in the EBD stages. One coupler is a commercial coupler and the other one, designed by the authors, has more S parameter stability in the frequency domain than the commercial one. It is shown that by using the designed coupler in the front-end EBD stage more stable isolation bandwidth and 45% better isolation value at ultra-wideband range of 1.5-3.5GHz are obtained, in comparison when using the commercial one.**

Keywords—duplexers, in-band full duplex, self-interference cancellation, couplers, antennas

I. INTRODUCTION

In-band full-duplex (IBFD) systems can theoretically double link capacity of Time Division Duplex (TDD) and Frequency Division Duplex (FDD) systems thus allowing simultaneous transmission and reception on the same frequency and reduce wireless latency [1], [2]. Transmitting and receiving on the same time-frequency resource results in strong co-channel Self-Interference (SI), which can be more powerful than the desired receive signal [2]. Any residual SI, due to unsuitable transmit (Tx) to receive (Rx) isolation, will effectively increase the receiver noise floor therefore reduces the capacity of the receive channel [3].

Existing IBFD designs [4], [5] involve various combinations of analog cancellation, digital cancellation, and antenna based suppression to provide the required isolation. Digital cancellation [6] cannot properly prevent SI from overloading the receiver. Analog cancellation [5], [6], can provide significant isolation and prevents receiver overloading in most cases [5]. Antenna based suppression and separation methods can provide significant isolation also, however these designs require additional antennas [6]. Single antenna full duplex systems in [5] use circulators to provide some level of Tx-Rx isolation but these are unattractive options due to their cost, size, and limited bandwidth. New duplexers based on SI Cancellation (SIC) at the receiver have received substantial interest to enable IBFD operation [1], [5]–[8].

This research is supported in part by the UK Engineering and Physical Sciences Research Council (EP/K503824/1), and in part by u-blox AG.

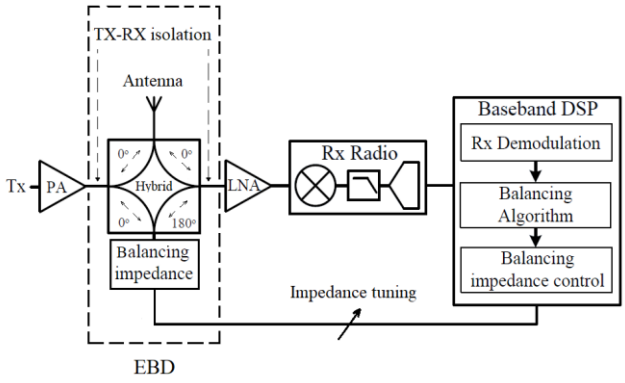

Fig. 1. EBD stage of IBFD system with adaptive balancing impedance

Recent results [3], [7], [9]–[11] have demonstrated that Electrical Balance Duplexers (EBDs), which is of interest as the first stage of passive Radio Frequency (RF) front-end cancellation in IBFD transceivers, implement a form of SIC in order to provide high transmit to receive isolation whilst facilitating simultaneous transmission and reception from a single antenna. EBD could potentially be combined with analog cancellation, digital cancellation, and full duplex MIMO technology [4]. The analog circuit technique of EBD works by coupling the transmitter, receiver and antenna using a four-port hybrid junction, along with a balancing impedance connected to the fourth port, Fig. 1. Using a suitable hybrid coupler, a high transmit-to-receive isolation is expected in the EBD stage when the balancing impedance is equal to the antenna impedance at all frequencies within the aimed bandwidth. However, in practice, the antenna impedance is not an ideal 50 Ω resistor but has a complex impedance having real and imaginary parts. This exhibits variations with respect to frequency so the bandwidth and value of the Tx-Rx isolation will be limited by the impedance mismatching between the antenna and balancing impedance.

Measured real antenna data in [3], [8], and results for a prototype EDB in [12], demonstrate that the variation in antenna impedance significantly reduces the isolation bandwidth. Evaluations that include measured antenna data in the EBD in [7], [9], [11] shows a mean isolation of 35 dB over a 20-MHz bandwidth at 1.9 GHz but poor performance of wider bandwidths, again said because of antenna impedance variations. A Micro- ElectroMechanical Systems (MEMS) implementation of tuneable balancing impedance of the EBD is presented in [13], balancing at 800 MHz and 1900 MHz to provide 43 dB isolation over a 20 MHz bandwidth at each frequency but introduce non-linear distortion into the system. Consequently, to maintain Tx-Rx isolation, the balancing

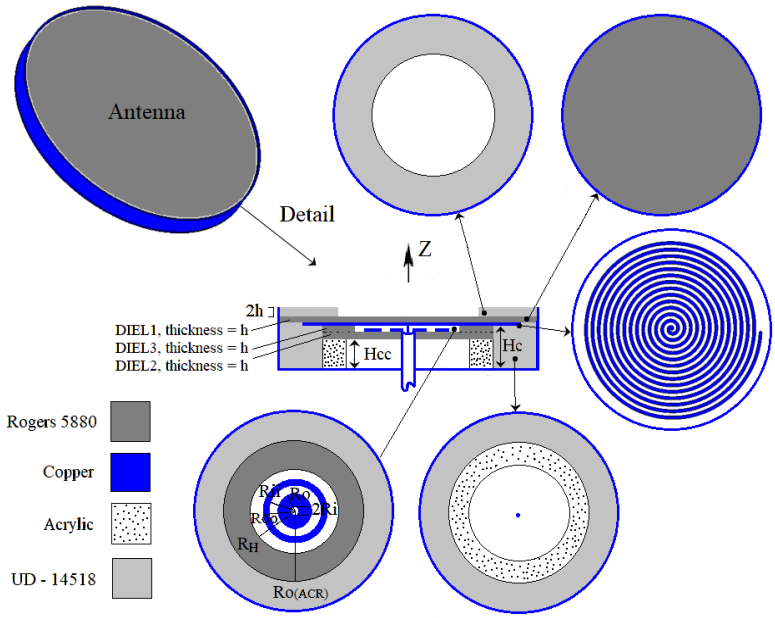

Fig. 2. Designed antenna with stable impedance, Section III.A (whole and cross-section views),

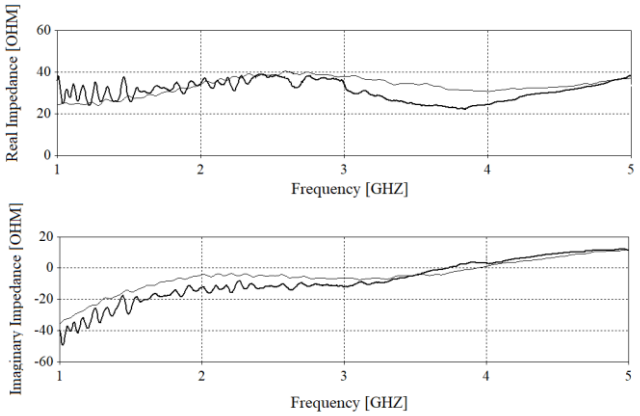

Fig. 3. Measured and simulated impedance of the antenna in Fig. 2.

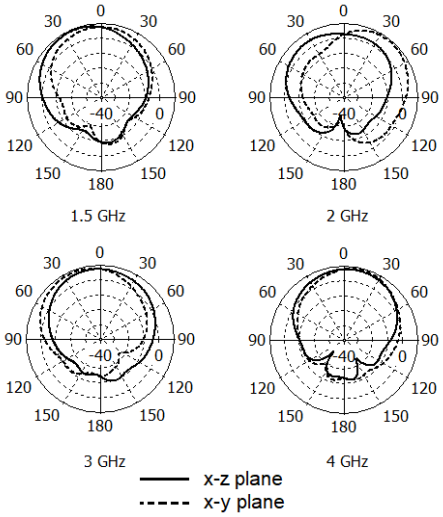

Fig. 4. Measured directivity pattern of the antenna in Fig.2.

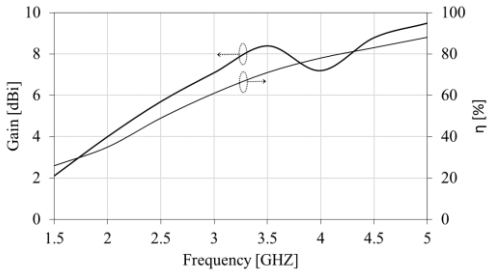

Fig. 5. Measured gain and radiation efficiency of the antenna in Fig. 2.

impedance must be tuneable as it tracks and mimics the antenna impedance as it changes. This requires an adaptive architecture [9], [11], Fig. 1, using a balancing algorithm which extremely limits both the mimic and the isolation bandwidths.

In all above scenarios in the literature, analyses consider the antenna impedance variations as the main factor limiting the SIC when the antenna is connected to a hybrid coupler. The main aim in this work is to investigate how the EBD isolation is affected by stability of coupler S parameters in the frequency domain. In the rest of this paper, in Section II, Tx-Rx gain function of EBD circuitry is briefly reviewed to assess EBD isolation in generic form. Used devices in the experiments of this work (stable impedance antenna, stable S parameter coupler, commercial coupler, and balancing load) are introduced in Section III. Stable impedance antenna and stable S parameter coupler are designed by authors. In Section IV, EBD isolations are measured when the two couplers are connected to the stable impedance antenna in two separate experiments. In comparison when using the commercial coupler in the EBD, it is shown that the EBD isolation bandwidth is increased, and the isolation value is optimized when using the designed coupler with higher S parameter stability. Finally, a conclusion is given in Section V.

II. Tx-Rx Gain of Electrical Balance Duplexers

Tx-Rx gain of an symmetrical EBD is given [10] by:

$$G_{Tx-Rx}(\omega) = L\,|\Gamma_{BAL}(\omega) - \Gamma_{ANT}(\omega)|^2. \qquad (1)$$

where Γ_{BAL} and Γ_{ANT} are the complex reflection coefficients of the balancing impedance and antenna impedance,

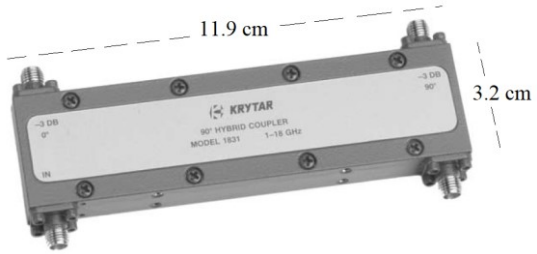

Fig. 6. Commercial 3-dB coupler, Model Krytar1831 [18] (Section III. B)

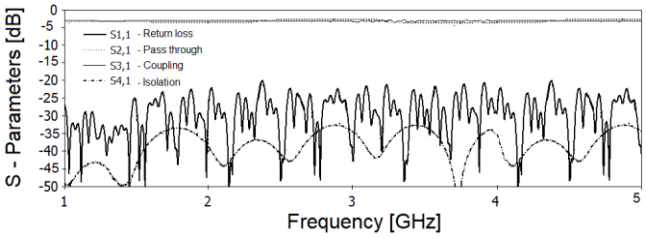

Fig. 7. Measured S parameters of the 3- dB Krytar1831 coupler in Fig. 6 (Section III. B).

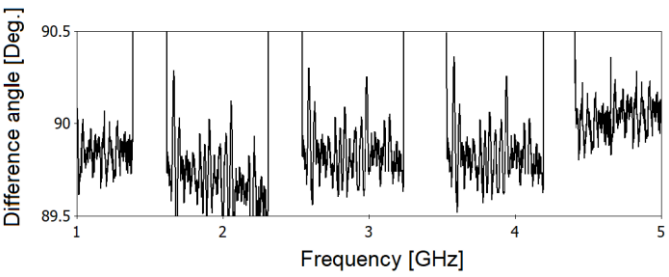

Fig. 8. Measured phase characteristic of the 3-dB Krytar1831 coupler in Fig. 6 (Section III. B), Zoomed view

respectively (see Fig.1), and for an ideal (lossless) hybrid L = ¼. As we can see from (1), the Tx-Rx gain is theoretically zero when the balancing reflection coefficient and antenna reflection coefficient are equal at the carrier frequency. To obtain maximum (theoretically infinite) Tx-Rx isolation over a given frequency band, the balancing impedance must be equal to the antenna impedance at all frequencies within that band such that $\Gamma_{BAL}(\omega) = \Gamma_{ANT}(\omega)$ for $\omega_l < \omega < \omega_h$ where ω_l and ω_h are the lower and upper limits of the band of interest, respectively. Also, coupler characteristics is a determining parameter to calculate the Tx-Rx gain. Results in [10] demonstrate that (1) remains valid for non-ideal circuit.

III. Devices

In this section, four RF elements used in the paper experiments are introduced. First device is an antenna with a stable impedance. More details about the antenna design are given in the authors other papers in [14] and [15]. Also, two couplers are introduced here, first one is a commercial coupler, and the second coupler is designed by the authors. The second coupler has more S parameter stability in the frequency domain than the first one. More details about design procedure of the second coupler are given in author's separate paper. Also, a wide band 50-ohm RF load is used as the balancing impedance.

A. Antenna with Stable Impedance - Designed

A single arm Archimedean Spiral (AS) is backed by a cavity, Fig. 2, to have an antenna with a unidirectional beam. The AS is formed as a conducting spiral strip arm of width w =2 mm on bottom of a disc shaped Rogers RT 5880 substrate - so called DIEL1- of radius A_C = 62 mm with a dielectric constant of ε_r = 2.2, loss tangent of 0.0009, h=0.79-mm thickness plus a 9 μm copper coating. DIEL1 has no copper on the top. The centerline of the spiral arm is defined by the function of $r = K\Phi$, where K is a constant and Φ is the winding angle, ranging from starting angle $\Phi_S = 0.07\pi$ Rad to ending angle $\Phi_E = 28\pi$ Rad. The antenna circumference C is defined by $C = 2\pi R_{max}$ with $R_{max} = K \Phi_E$ where K = 0.64 mm/rad, R_{max}= 56 mm. The cavity radius, A_C, has 6 mm distance from the arm end to the cavity wall as A_C = 62 mm= 0.31 λ_L whilst λ_L is the wavelength at the lowest design frequency of 1.5 GHz. The distance between the bottom of the cavity and the spiral on the bottom of DIEL1 substrate is considered as H_C = 6.9 mm = 0.035 λ_L. The height of the copper case wall is chosen as H_C + 2h to surround the DIEL1 disc substrate while the case has a 1 mm uniform thickness of copper.

Reflected fields from bottom of the case are attenuated in the designed antenna using electromagnetic absorbers (EMAs) made up of model UD-14518 of ARC Technology to make the antenna impedance more stable in an UWB frequency range. The UD-14518 specified by relative permittivity of $\varepsilon_r = \varepsilon' - j\varepsilon'' \sim 22+3j$ and relative permeability of $\mu_r = \mu' - j\mu'' \sim 4.5+2j$ at aimed the bandwidth [16]. As shown in Fig. 2, a ring-shaped Electromagnetic Absorber (EMA) strip - so called EMA1- of optimized width 11mm and with the same height of copper case H_c = 6.9 mm is placed under the antenna arms. Also, second EMA, so called EMA2, is added to above the DIEL1 substrate to more improve impedance stability. EMA2 has an optimized thickness of 2h = 1.6 mm while its outer radius is equal to the cavity diameter of A_C and its inner radius is A_C -17mm = 45mm.

A capacitive impedance matching using two cocentric planar copper rings, Fig. 2, is also used to improve impedance stability. Maximum bandwidth for a stable impedance is achieved when air with dielectric constant of ε_r =1 is considered between the copper rings and the spiral. As seen, the two cocentric planar copper rings are considered on the top surface of a disc shape dielectric material, so called DIEL2, with a distance of h = 0.79 mm between the copper rings and the spiral body. DIEL2 with a thickness of h is made up of the same material of Rogers RT 5880. DIEL2 has a small hole with R_i = 1.7mm radius in the centre for passing the coaxial cable whilst the outer radius of DIEL2 is 41mm. Also, a planar dielectric ring, so called DIEL3, with the same thickness and the same material with DIEL2 is used as a spacer between DIEL2 and DIEL1. DIEL3 has a hole with radius of R_H = 35mm in the centre whilst its outer radius is equal with the outer radius of DIEL2. The internal copper ring has inner radius of R_i=1.7mm and outer radius of R_O= 5.5 mm while the external ring has inner radius of R_{ii} = 8mm and outer radius of R_{OO} =11 mm. To hold the substrates and spiral a cylindrical ring is 3D printed on Acrylic material with a dielectric constant of $\varepsilon_{r(ACR)}$ = 3.5, internal radius of R_{iA} = of 41 mm, outer radius of R_{oA} = 51 mm and height of $H_{CC} = H_C$ -2h = 5.3mm. The antenna is fed by a 50 Ω coaxial cable whereas the inner conductor of the cable is connected to the AS at its starting angle and outer ground conductor of the cable is connected to the inner radius of internal capacitive ring at the top surface of DIEL3.

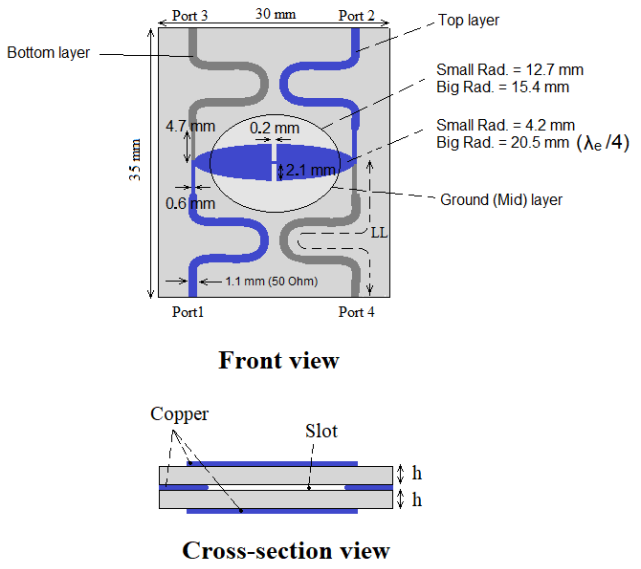

Fig. 9. Designed 3-dB coupler with stable S parameter (Section III. C)

The Finite Integration Technique (FIT) with high meshing in CST MICROWAVE STUDIO [17] software is used for simulations. Measured and simulated antenna impedances with a stable impedance at 1.5 GHz to 3.5 GHz range are shown in Fig. 3, with an average variation of about 15 Ω for the measured imaginary and real impedance. Also, measured directivity pattern of the antenna and its measured gain/efficiency vs frequency plots are shown respectively in Fig. 4 and Fig. 5. The antenna has a measured Axial Ratio (AR) below 3 dB indicating a circular polarization over 1.6 GHz (AR plot is not shown here). These results indicate good impedance stability at 1.5 - 3.5 GHz range for the designed antenna while the antenna also has a suitable radiation performance at this Ultra-wide Band (UWB) bandwidth. The fabricated antenna is shown in Section IV.

B. Commercial 3-dB Coupler (Krytar Model 1831)

Krytar coupler model 1831 is an UWB commercially available coupler [18], Fig. 6. Measurement results of the coupler by Vector Network Analyzer (VNA) are given in Fig. 7 and Fig. 8. As seen, this commercial coupler features UWB characteristics with the coupling of 3 ± 1 dB at 1-5 GHz bandwidth. Also, isolation in the order of better than 30 dB and return loss in the order of better than 20 dB are measured. It is seen that the measured S parameters are not very stable in the frequency domain as there are dense variations around 15 dB for isolation and 25 dB for return loss at 1-3.5 GHz range. In Fig. 8, it is observed that the measured phase difference between output ports is dominantly around 90° over the bandwidth, needed for a suitable quadrature hybrid coupler.

C. 3-dB coupler with Stable S Parameter - Designed

Proposed miniaturized coupler capable of providing tight coupling over an UWB band, is shown in Fig. 9 where its coupling mechanism is similar to [19] and [20]. The differences for the proposed model concern the shaping factor of the broadside coupled strips, the slot, electrical size and most importantly the operation frequency which is in the ultra-high frequency band. This coupler consists of three conductor copper layers which are interleaved by two dielectric substrates. The top copper layer includes ports 1 and 2. The

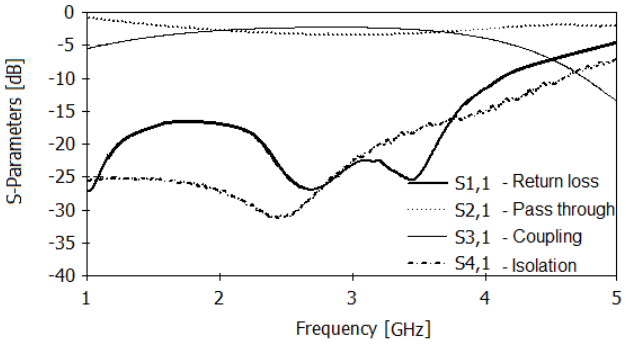

Fig. 10. Fig. 7. Measured S parameters of the designed 3-dB coupler with stable S parameter in Fig. 9 (Section III. C).

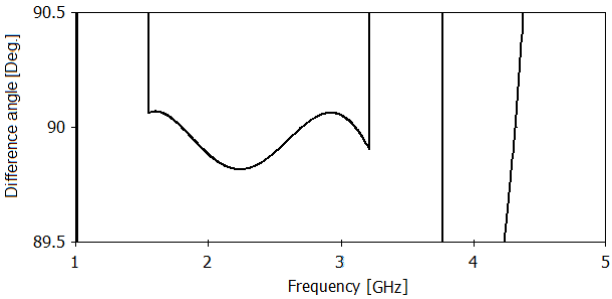

Fig. 11. Measured phase characteristic of the designed 3-dB coupler with stable S parameter in Fig. 9 (Section III. C), Zoomed view

Fig. 12. Wideband 50-ohm RF Load (Section III. D)

bottom copper layer is similar to the top layer, but the ports here are ports 3 and 4. Ports 3 and 4 are on opposite sides of the substrate compared to ports 1 and 2. The two layers are coupled via a slot, which is made in the copper layer supporting the top and bottom dielectrics. As seen in Fig. 9, the two microstrip conductors and the slot are of an elliptical shape. The 50 Ω microstrip lines are included to make connections to SMA ports. The structure features double symmetry with respect to both horizontal and vertical plans.

Analysis starts in a similar way to the ones described in [21] for the equivalent rectangular shaped microstrips. If characteristic impedance of the microstrip ports of the coupler is $Z_0 = 50\,\Omega$ and the coupling factor is $C_{dB} = 3$ dB, the values of even mode characteristic impedance Z_{ev} and odd mode characteristic impedance Z_{od} are calculated as 175.5 Ω and 14.2 Ω, respectively.

The validity of the presented design is tested in the 1.5–3.2 GHz frequency band where the centre frequency of operation is 2.35 GHz. A Rogers RO4350B substrate with a dielectric constant of 3.48 and a loss tangent of 0.0037, h = 0.51mm thickness, plus 35- μm-thick conductive copper is used for the coupler development. The elliptical body length is chosen as 20.5 mm ~ $\lambda/6$ ~ $\lambda_e/4$ where λ_e is effective wavelength and λ is free space wavelength at the central frequency of 2.35 GHz. The return loss, coupling, and isolation of the designed coupler are first verified by running high mesh FIT in the CST software and the final obtained dimensions are shown in Fig. 9.

Four phase shifters each having length of LL = 33 mm= 0.4 λ_e are added to the terminals of elliptical bodies to adjust output phase difference to 90º, needed for a suitable quadrature hybrid coupler, Fig. 9. To maintain a compact size, phase shifters are formed as curved microstrip lines. Simulations do not show considerable differences in results when the curves angle are not smaller than 75 degree. A combination of impedance matching technique and structural modifications also have been employed to optimize the coupler results. The impedance matching is carried out in a similar way for all four ports by narrowing the width of tracks which connect the ports to the elliptical body as shown in Fig. 9. Also, two narrow slots have been etched on each elliptical body as shown in the same figure. Measurement results by VNA are given in Fig. 10 and Fig. 11. The coupler features measured UWB characteristics with coupling of 3 ± 1 dB at the aimed 1.5-3.2 GHz band. Also, smooth isolation in the order of better than 25 dB and return loss in the order of better than 17 dB is achieved as there are non-dense variations around 10 dB for isolation and 9 dB for return loss at 1-3.5 GHz range. It is seen that the S parameters for the designed coupler have less variation density and more stability in the frequency domain in comparison with the commercial Krytar 1831 in Section III.B. It is observed in Fig. 11 that the measured phase difference between ports 2 and 3 is about 90º over the target band. The fabricated coupler is shown in Section IV. These results indicate that this compact coupler with 35 mm × 30 mm × 1.1 mm (0.27 λ× 23 λ× 0.009λ) dimension operates as a backward wave quadrature coupler.

D. Wideband 50-ohm RF Load

A wideband commercial 50-ohm RF load (Fig. 12) - which has the nearest commercially available impedance to the antenna impedance - is used in the experiments.

IV. Tx-Rx Isolation in EBD Stage and Comparisons

In this section Tx-Rx isolations of EBD are investigated when the devices introduced in Section III are used and the obtained results are compared together. The designed stable impedance antenna (Section III.A) is connected to the commercial Krytar 1831 hybrid coupler (Section III.B) and stable S parameter coupler (Section III.C) in two separate experiments to from EBD, Fig. 13. For the Krytar 1831 coupler from Fig. 7 it is seen that the measured S parameters are not stable in the frequency domain at 1-3.5 GHz range as there are dense isolation variations around 15 dB and return loss variations around 25 dB while for the designed coupler (Fig. 10) there are less dense variations with the isolation variations around 10 dB and return loss variations around 9 dB. A 50 Ω wideband 50-ohm RF load (Section III.D) is also connected as balancing impedance to both couplers. The experiment setups are shown in Fig. 14.

Average isolation of 20 dB and 29dB are measured by VNA at 1.5GHz-3.5GHz bandwidth respectively for EBD with the Krytar 1831 coupler and EBD with the designed stable S parameter coupler, Fig. 13. While both EBDs use the same antenna and the same 50 Ω RF load, it is seen that when using the designed coupler more stable UWB bandwidth and 45% better isolation value are obtained in comparison when using the Krytar 1831 coupler.

First reason of variations and limitations still seen in the obtained optimized UWB isolation could be the small inherent impedance variations of the designed coupler and the antenna.

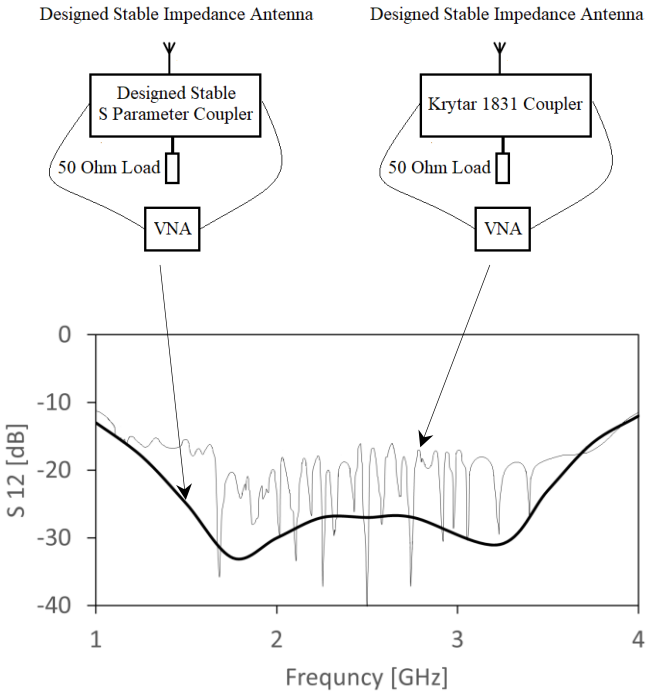

Fig. 13. Measured Tx-Rx EBD isolation when using designed stable impedance antenna with the commercial Krytar 1831 coupler and the designed stable S parameter coupler

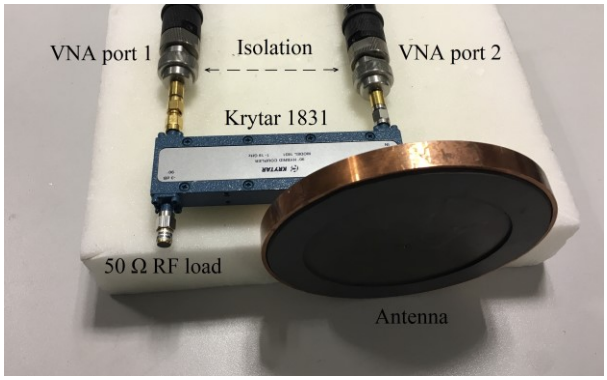

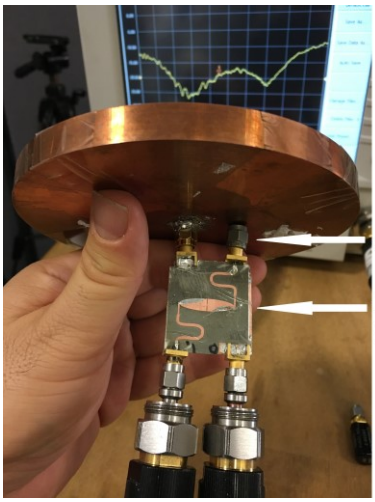

Fig. 14. EBD Setup to measure Tx-Rx isolation when the designed stable impedance antenna is connected to: (Top) Krytar 1831 hybrid coupler (Below) Designed stable S parameter coupler.

The second reason could be impedance mismatch between antenna and 50 Ω balancing load.

V. Conclusion

Electrical Balance Duplexers (EBDs) in In-Band Full Duplex (IBFD) transceivers, isolates transmit and receive signals to implement a form of self-interference cancellation to facilitates simultaneous communication from single antenna. EBD works by coupling transmitter, receiver, antenna, and balancing impedance using a hybrid coupler. The balancing impedance in the EBD needs to be equal as much as possible to the antenna impedance to achieve a high isolation where the antenna impedance variations limit the isolation bandwidth. Hybrid couplers are also not ideal elements, and their S parameters are variable in the frequency domain. An antenna with a stable impedance, designed by authors, has been connected to two different hybrid couplers in the EBD stages. One coupler is commercial Krytar model 1831 and the other one, designed by authors, has more S parameter stability in the frequency domain. It is shown that using hybrid coupler with more stable isolations results to higher isolation bandwidth and better isolation value in the EBD stage at an UWB frequency range from 1.5 GHz to 3.5 GHz.

References

[1] L. Laughlin *et al.*, "Tunable Frequency-Division Duplex RF Front End Using Electrical Balance and Active Cancellation," *IEEE Transactions on Microwave Theory and Techniques*, vol. 66, no. 12, pp. 5812–5824, 2018.

[2] S. N. Venkatasubramanian, C. Zhang, L. Laughlin, K. Haneda, and M. A. Beach, "Geometry-Based Modeling of Self-Interference Channels for Outdoor Scenarios," *IEEE Transactions on Antennas and Propagation*, vol. 67, no. 5, pp. 3297–3307, 2019.

[3] L. Laughlin, M. A. Beach, K. A. Morris, and J. L. Haine, "Optimum single antenna full duplex using hybrid junctions," *IEEE Journal on Selected Areas in Communications*, vol. 32, no. 9, pp. 1653–1661, 2014.

[4] E. Aryafar, M. Khojastepour, K. Sundaresan, S. Rangarajan, and M. Chiang, "MIDU: Enabling MIMO full duplex," in *Proc. ACM Int. Conf. Mob. Comput. Netw*, 2012, pp. 257–268.

[5] D. Bharadia, E. McMilin, and S. Katti, "Full duplex radios," in *Proc. ACM SIGCOMM,* 2013, pp. 375–386.

[6] M. Duarte, C. Dick, and A. Sabharwal, "Experiment-driven characterization of full-duplex wireless systems," *IEEE Transactions on Wireless Communications*, vol. 11, no. 12, pp. 4296–4307, 2012.

[7] L. Laughlin, C. Zhang, M. A. Beach, K. A. Morris, and J. Haine, "A widely tunable full duplex transceiver combining electrical balance isolation and active analog cancellation," in *IEEE 81st Veh. Tech. Conf.*, 2015, vol. 2015, pp. 1–5.

[8] B. Debaillie *et al.*, "Analog/RF solutions enabling compact full-duplex radios," *IEEE Journal on Selected Areas in Communications*, vol. 32, no. 9, pp. 1662–1673, 2014.

[9] L. Laughlin, C. Zhang, M. A. Beach, K. A. Morris, and J. L. Haine, "Passive and active electrical balance duplexers," *IEEE Transactions on Circuits and Systems II: Express Briefs*, vol. 63, no. 1, pp. 94–98, 2016.

[10] S. H. Abdelhalem, P. S. Gudem, and L. E. Larson, "Hybrid transformer-based tunable differential duplexer in a 90-nm CMOS process," *IEEE Transactions on Microwave Theory and Techniques*, vol. 61, no. 3, pp. 1316–1326, 2013.

[11] L. Laughlin, M. A. Beach, K. A. Morris, and J. L. Haine, "Electrical balance duplexing for small form factor realization of in-band full duplex," *IEEE Communications Magazine*, vol. 53, no. 5, pp. 102–110, 2015.

[12] B. Van Liempd, J. Craninckx, R. Singh, P. Reynaert, S. Malotaux, and J. R. Long, "A dual-notch +27dBm Tx-power electrical-balance duplexer," in *European Solid-State Circuits Conference*, 2014, pp. 463–466.

[13] C. Zhang, L. Laughlin, M. A. Beach, K. A. Morris, and J. L. Haine, "Micro-electromechanical impedance control for electrical balance duplexing," in *Europ. Wireless Conf.*, 2016, pp. 263–268.

[14] S. Soodmand, M. A. Beach, and K. A. Morris, "Small Antenna with Stable Impedance and Circular Polarization," in *IEEE 15th European Conference on Antennas and Propagation (EuCAP)*, 2021.

[15] S. Soodmand, K. Morris, and M. Beach, "Quantization of Impedance Stability in Frequency Domain," in *IEEE International Electrical Engineering Congress (iEECON2021)*, 2021.

[16] "[Online]. Available." https://www.hitek-ltd.co.uk/index.php/downloads/dl/file/id/9822/product/0/ud_14518_rev_b_8ghz_urethane_1_14mm.pdf.

[17] "CST Studio Suite Electromagnetic Field Simulation Software (2020)." DASSAULT SYSTÈMES, [Online]. Available: https://www.3ds.com/products-services/simulia/products/cst-studio-suite/.

[18] "Krytar 1831 - Datasheet." https://krytar.com/pdf/1831.pdf.

[19] T. Tanaka, K. Tsunoda, and M. Aikawa, "Slot—coupled directional couplers on a both—sided substrate MIC and their applications," *Electronics and Communications in Japan (Part II: Electronics)*, vol. 72, no. 3, 1989.

[20] A. M. Abbosh and M. E. Bialkowski, "Design of compact directional couplers for UWB applications," *IEEE Transactions on Microwave Theory and Techniques*, vol. 25, no. 22, pp. 189–194, 2007.

[21] M. F. Wong, V. Fouad Hanna, O. Picon, and H. Baudrand, "Analysis and design of slot-coupled directional couplers between double-sided substrate microstrip lines," in *IEEE MTT-S International Microwave Symposium Digest*, 1991, pp. 2123–2129.